ISA Transactions 84 (2019) 214–224

Contents lists available at ScienceDirect

ISA Transactions

journal homepage: www.elsevier.com/locate/isatrans

Practice article

Design and implementation of continuous finite-time sliding mode control for 2-DOF inertially stabilized platform subject to multiple disturbances

Jianliang Mao, Shihua Li *, Qi Li, Jun Yang

Key Laboratory of Measurement and Control of Complex Systems of Engineering, Ministry of Education, School of Automation, Southeast University, Nanjing, Jiangsu 210096, People's Republic of China

HIGHLIGHTS

- Multiple disturbances are estimated and compensated without complex modeling work.
- Finite-time convergence of the inertial angular rate tracking error is guaranteed.
- Control chattering is alleviated remarkably due to continuous control actions.

ARTICLE INFO

Article history:
Received 13 March 2017
Received in revised form 4 August 2018
Accepted 14 September 2018
Available online 12 October 2018

Keywords:
Inertially stabilized platform
Finite-time disturbance observer
Continuous finite-time sliding mode control
Super-twisting algorithm
Chattering attenuation

ABSTRACT

Control performances of inertially stabilized platforms (ISPs) are always affected by various disturbed phenomena such as cross-couplings, mass unbalance, parameter variations, and external disturbances in real applications. To improve the dynamic response and the disturbance rejection ability of the ISP, a continuous finite-time sliding mode control (SMC) approach with cascaded control structure is proposed. By constructing a finite-time disturbance observer, the multiple disturbances are precisely estimated in real time without the complex modeling and calibration work. Under the field oriented control framework, for the stabilized loop subsystem, an improved super-twisting controller incorporating the disturbance estimates is developed whereas for the current loop subsystem, the super-twisting control method is directly employed. Finite-time convergence of the inertial angular rates is guaranteed with the continuous control action such that chattering is alleviated remarkably. Moreover, by utilizing the manner of disturbance compensation, the feedback control gains can be tuning down without sacrificing the disturbance rejection ability. Comparative experiments are performed to verify the effectiveness of the proposed control approach.

1. Introduction

Optical–electronic tracking system has been playing an important role in scientific, military and commercial applications, such as missile guidance, target tracking, environmental monitoring, astronomical telescopes, etc [1,2]. Due to the existence of vehicle motion or vibration, it is extremely a challenging task to maintain the orientation of the sensor toward a moving target. To this end, inertially stabilized platforms (ISPs) are commonly adopted to keep the line-of-sight (LOS) steady relative to the inertial space. In order to realize the high performance with fast dynamic response and high tracking precision for the ISP system, numerous advanced control approaches instead of the traditional proportional–integral (PI) controller have been put forward, such as H∞ control [3,4], fuzzy control [5,6], internal mode control [7], and neural networks control [8,9]. However, as a multiple degree-of-freedom (DOF) electromechanical device, the ISP is essentially a complicated nonlinear system, which is subject to the various disturbed phenomena such as cross-couplings, mass unbalance, and parameter variations [2,10]. Moreover, it may also suffer from the side effects caused by the wind stream when mounted outside the vehicle [11]. As such, there are some limitations in disturbance rejection when applying the aforementioned approaches in high-precision applications. For instance, the non-vanishing external disturbances considered therein can only be attenuated to some extent rather than removed completely when the disturbance assumption is violated. In addition, in order to reject the effects

* Corresponding author.
E-mail address: lsh@seu.edu.cn (S. Li).

https://doi.org/10.1016/j.isatra.2018.09.014
0019-0578/

Nomenclature

{B},{K},{A}	Base frame, yaw gimbal frame, and pitch gimbal frame, respectively
x_b, y_b, z_b	Coordinate axes of the frame {B}
x_k, y_k, z_k	Coordinate axes of the frame {K}
x_a, y_a, z_a	Coordinate axes of the frame {A}
p_b, q_b, r_b	Roll, pitch, and yaw components of the inertial angular rate vector expressed in the frame {B}, respectively
p_k, q_k, r_k	Roll, pitch, and yaw components of the inertial angular rate vector expressed in the frame {K}, respectively
p_a, q_a, r_a	Roll, pitch, and yaw components of the inertial angular rate vector expressed in the frame {A}, respectively
v_1	Rotational angle from the frame {B} to the frame {K} about the z_b-axis
v_2	Rotational angle from the frame {K} to the frame {A} about the y_k-axis
$\boldsymbol{R_b^k}$	Rotation matrix from the frame {B} to the frame {K}
$\boldsymbol{R_k^a}$	Rotation matrix from the frame {K} to the frame {A}
T_q	Total external torque about the y_a-axis of pitch gimbal
T_r	Total external torque about the z_k-axis of yaw gimbal
$l = 1, 2$	Parameters related to the yaw and pitch gimbals, respectively
T_{cl}	Cross-coupling torque
T_{el}	Electromagnetic torque
f_l	External disturbance torque
B_l	Viscous friction coefficient
F_l	Lumped uncertainty
J_{ol}	Nominal value of the total moment of inertial
i_{dl}, i_{ql}	d-axis and q-axis stator currents, respectively
i_{dl}^*, i_{ql}^*	Desired d-axis and q-axis stator currents, respectively
L_{dl}, L_{ql}	d-axis and q-axis inductances, respectively
u_{dl}, u_{ql}	d-axis and q-axis stator voltages, respectively
R_{sl}	Stator resistance
n_{pl}	Number of pole pair
ϕ_{vl}	Rotor flux linkage
K_{fl}	Thrust coefficient

caused by considerable cross-couplings, the precise feedback linearization in [7,8] does not seem to be an appropriate way since the uncertain couplings are difficult to model accurately, especially in the presence of mass unbalance and parameter uncertainties [12]. Consequently, how to eliminate the influences induced by the multiple disturbances in the ISP system is a significant topic in practical applications [13].

Sliding mode control (SMC) provides an alternative way to deal with system uncertainties and external disturbances, which has been widely used in guidance and tracking system [14]. While treating the adverse effects as the lumped uncertainties, the SMC appears to be a simple and effective way to reject the disturbances [15]. Yet the limitation is the presence of the discontinuous control action due to the switching strategy [16]. To reduce the chattering phenomena, a common solution is to replace the switching function sign(σ) with some saturation or sigmoid functions. Unfortunately, it can only make the system states converge to the neighborhood

of the equilibrium point, which is apparently not suitable for the high precision control of the ISP system. Continuous sliding mode control (CSMC) is proposed via many effective methods to solve the problem [17–20]. It has been reported in [17,18] that finite time control (FTC) method associating with the nonsingular terminal sliding mode (NTSM) can realize the continuous action. However, the tracking error cannot be guaranteed to reach the origin in the presence of model uncertainties and external disturbances. In recent years, another approach named as high-order sliding mode control (HOSMC) [19,20] is extensively studied, in which the super-twisting (STW) algorithm is proved to be efficient in disturbance rejection and convenient for implementation on the system with relative degree one [21]. This advantage seems to be adequate for the cascade control structure of the ISP (i.e., tracking loop, stabilized loop, and current loop). However, the conventional STW controller requires the knowledge of the boundary of disturbance as well as its derivative [20], which is hard to obtain as a priori in the ISP system due to the unknown cross-couplings and external disturbances. Generally, larger control gains are required for the possibly larger robustness region, but this will lead to the undesirable dynamic performances such as the severe steady-state fluctuations due to measurement noise amplification.

A practical and reliable means for reducing the feedback control gains is to perform disturbance estimation and compensation [22]. As is well known, if the disturbance is the slow time-varying or constant one, it can be precisely estimated by a convenient approach named as the extended state observer (ESO) [23,24]. But for the estimation of fast time-varying disturbances such as cross-couplings in ISP systems, the estimation errors can only be ensured to converge to a bounded region rather than the origin [25]. Finite-time disturbance observer (FTDO) introduced in [26,27] is known as an efficient way to estimate the disturbances with any continuously differentiable types. With this feature in mind, the design manner can be possibly borrowed for the estimation of the mentioned multiple disturbances.

To eliminate the undesirable influences caused by the multiple disturbances in the ISP system, this paper explores a continuous finite-time sliding mode control approach. The adopted 2-DOF servo mechanism is composed of two permanent magnet synchronous motors (PMSMs). First, the dynamic model taking into account cross-couplings, mass unbalance, parameter variations, and external disturbances is established. By treating the multiple disturbances as the lumped uncertainty, the cross-coupled ISP system is taken to be decoupled. Then, under the field oriented control (FOC) framework, for the stabilized loop subsystem, an improved STW (IMSTW) controller incorporating the disturbance estimates is developed and for the current loop subsystem, the convenient STW control is directly employed. On the basis of Lyapunov stability theory, a global finite-time stability analysis is given for the closed-loop system. Compared with the existing methods, the proposed control scheme exhibits the following attractive features:

(1) By constructing the FTDO, the multiple disturbances arising from various disturbed phenomena in the ISP system can be precisely estimated in real time without the complex modeling and calibration work.
(2) Global finite-time convergence of the output tracking error is guaranteed with continuous control action such that the control chattering is substantially alleviated.

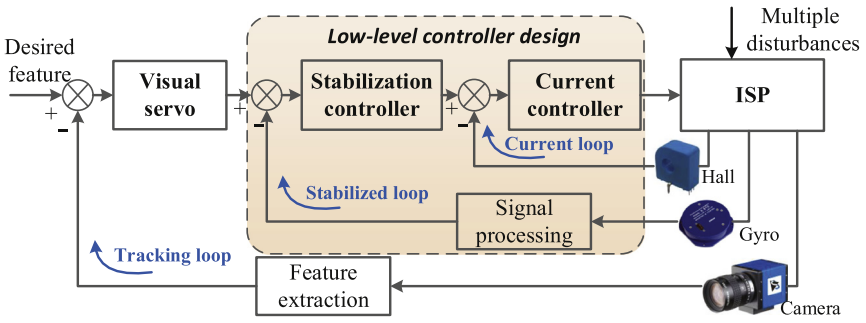

Fig. 1. Control framework of the optical–electronic tracking system.

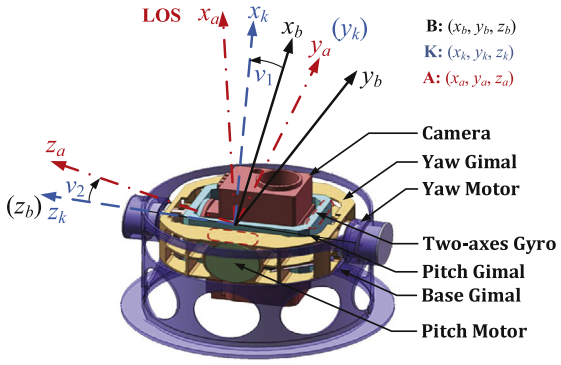

Fig. 2. 2-DOF ISP configuration diagram.

(3) Thanks to the disturbance feedforward compensation, the feedback control gains can be reduced without sacrificing the disturbance rejection ability as opposed to the conventional STW control.

The proposed algorithm is verified on the experimental platform with a digital signal processor (DSP) model TMS320F28335.

2. Model description

As shown in Fig. 1, the control framework of the optical-electronic tracking system is generally composed of three feedback control loops, i.e., tracking loop, stabilized loop, and current loop [2]. To improve the dynamic response and the disturbance rejection ability of the ISP, we focus on the controllers design of the stabilized loop and the current loop in this paper. The issue of the outer (visual servo) control-loop design is dealt in our another work. Before starting the discussions on ways to construct the feedback controllers, the dynamic model of the 2-DOF ISP is firstly to be established.

2.1. Dynamic model of 2-DOF gimbal

A typical configuration of the 2-DOF ISP system is shown in Fig. 2. By fixing a two-axes gyro on the pitch gimbal frame, the stable control of the LOS can be accomplished on both pitch and yaw channels. To begin with, three reference frames are introduced, i.e., the base frame {B}, the yaw gimbal frame {K}, and the pitch gimbal frame {A}, where $\{x_b, y_b, z_b\}$, $\{x_k, y_k, z_k\}$, and $\{x_a, y_a, z_a\}$ are the corresponding coordinates of the frames {B}, {K}, and {A}, respectively. All the center of rotation for three frames are assumed to be located in the coordinate origin.

For the angular rates of the frames {B}, {K}, and {A} relative to the inertial space, we introduce $\boldsymbol{\Omega_B}$, $\boldsymbol{\Omega_K}$, and $\boldsymbol{\Omega_A}$, respectively, where $\boldsymbol{\Omega_B} = [p_b, q_b, r_b]^{\mathrm{T}}$, $\boldsymbol{\Omega_K} = [p_k, q_k, r_k]^{\mathrm{T}}$, and $\boldsymbol{\Omega_A} = [p_a, q_a, r_a]^{\mathrm{T}}$. Then, the angular rate kinematics of two gimbals are given by

$$\boldsymbol{\Omega_K} = \boldsymbol{R_b^k} \cdot \boldsymbol{\Omega_B} + \begin{bmatrix} 0 \\ 0 \\ \dot{v}_1 \end{bmatrix}, \boldsymbol{\Omega_A} = \boldsymbol{R_k^a} \cdot \boldsymbol{\Omega_K} + \begin{bmatrix} 0 \\ \dot{v}_2 \\ 0 \end{bmatrix} \tag{1}$$

where

$$\boldsymbol{R_b^k} = \begin{bmatrix} \cos v_1 & \sin v_1 & 0 \\ -\sin v_1 & \cos v_1 & 0 \\ 0 & 0 & 1 \end{bmatrix}, \boldsymbol{R_k^a} = \begin{bmatrix} \cos v_2 & 0 & -\sin v_2 \\ 0 & 1 & 0 \\ \sin v_2 & 0 & \cos v_2 \end{bmatrix}. \tag{2}$$

Assume that the inertial matrices of two gimbals are denoted as

$$\boldsymbol{J_A} = \begin{bmatrix} J_{ax} & D_{xy} & D_{xz} \\ D_{xy} & J_{ay} & D_{yz} \\ D_{xz} & D_{yz} & J_{az} \end{bmatrix}, \boldsymbol{J_K} = \begin{bmatrix} J_{kx} & d_{xy} & d_{xz} \\ d_{xy} & J_{ky} & d_{yz} \\ d_{xz} & d_{yz} & J_{kz} \end{bmatrix}. \tag{3}$$

According to the Newton–Euler theory, the dynamic model of the pitch gimbal can be derived as

$$J_{ay}\dot{q}_a = T_q + T_{D1} + T_{D2} \tag{4}$$

where T_q is the total external torque about the pitch gimbal y_a-axis, T_{D1} is the disturbance caused by the base rotation, and T_{D2} is the cross-coupling term caused by the relative motion between the base and yaw gimbals, which are expressed by

$$\begin{aligned} T_{D1} &= -(D_{yz}\sin v_2 + D_{xy}\cos v_2)(\dot{p}_k + q_k r_k) \\ &\quad + (D_{yz}\cos v_2 - D_{xy}\sin v_2)p_k r_k \\ &\quad + [(J_{az} - J_{ax})\cos(2v_2) - 2D_{xz}\sin(2v_2)]p_k q_k \\ &\quad + \frac{1}{2}[(J_{az} - J_{ax})\sin(2v_2) + 2D_{xz}\cos(2v_2)]p_k^2, \\ T_{D2} &= (D_{xy}\sin v_2 - D_{yz}\cos v_2)\dot{r}_k \\ &\quad - \frac{1}{2}[(J_{az} - J_{ax})\sin(2v_2) + 2D_{xz}\cos(2v_2)]r_k^2. \end{aligned} \tag{5}$$

Likewise, the dynamic model of the yaw gimbal can be derived as

$$J_{km}\dot{r}_a = T_r + T_{d1} + T_{d2} + T_{d3} + T_{d4} \tag{6}$$

where T_r is the total external torque about the yaw gimbal z_k-axis, J_{km} is the total moment of inertia, T_{d1}, T_{d2}, and T_{d3} are the disturbances caused by the base rotation, and T_{d4} is the cross-coupling term caused by the relative motion between the yaw and

pitch gimbals, which are expressed by

$$\begin{aligned}
J_{km} &= J_{kz}\sec v_2 + J_{ax}\sin v_2\tan v_2 + J_{az}\cos v_2 - 2D_{xz}\sin v_2,\\
T_{d1} &= [J_{kx} + J_{ax}\cos^2 v_2 + J_{az}\sin^2 v_2\\
&\quad + D_{xz}\sin(2v_2) - (J_{ky} + J_{ay})]p_k q_k,\\
T_{d2} &= [(J_{ax} - J_{az})\cos(2v_2) + 2D_{xz}\sin(2v_2) - J_{ay} + J_{km}\cos v_2]\dot{v}_2 p_k\\
&\quad + J_{km}\sin v_2\dot{p}_k + [(J_{ax} - J_{az})\sin(2v_2) - 2D_{xz}\cos(2v_2)\\
&\quad + J_{km}\sin v_2]q_k r_k\\
&\quad + (D_{yz}\cos v_2 - D_{xy}\sin v_2)\dot{q}_k - (D_{yz}\sin v_2 + D_{xy}\cos v_2)q_k^2,\\
T_{d3} &= -[d_{xz} + (J_{az} - J_{ax})\sin v_2\cos v_2 + D_{xz}\cos(2v_2)](\dot{p}_k - q_k r_k)\\
&\quad - (d_{yz} + D_{yz}\cos v_2 - D_{xy}\sin v_2)(\dot{q}_k + p_k r_k)\\
&\quad - (d_{xy} + D_{xy}\cos v_2 + D_{yz}\sin v_2)(p_k^2 - q_k^2),\\
T_{d4} &= (D_{xy}\sin v_2 - D_{yz}\cos v_2)\dot{q}_a + (D_{xy}\cos v_2 + D_{yz}\sin v_2)q_a^2\\
&\quad + [(J_{az} - J_{ax})\sin(2v_2) + 2D_{xz}\cos(2v_2) - J_{km}\sin v_2]q_a r_k.
\end{aligned} \tag{7}$$

The detailed derivation process of the dynamics (4) and (6) can be referred to [12]. However, it is worth noting that the dynamic model (6) is slightly different from that in [12], which lies in that the output of the yaw channel is the inertial angular rate r_a rather than r_k, i.e., r_a is the system variable we want to control. Since r_k is related to r_a, we can further derive the dynamic model about r_a with the relationship $r_a = p_k\sin v_2 + r_k\cos v_2$. For this argument, one can refer to the specific explanation in [2].

Although the cross-couplings can be accurately modeled as (5) and (7), they are rather complex to be precisely compensated by using feedback linearization method since there are so many uncertain physical parameters as well as the unmeasured variables in the dynamics. For the sake of simplification, denoting the cross-couplings as $T_{c1} = T_{d1} + T_{d2} + T_{d3} + T_{d4}, T_{c2} = T_{D1} + T_{D2}$. Furthermore, taking into account the external disturbance $f = [f_1, f_2]^{\mathrm{T}}$ and the viscous friction torque, the dynamic models (4) and (6) can be rewritten in the compact form as

$$\begin{cases} J_{km}\dot{r}_a = T_{e1} - B_1\dot{v}_1 - T_{c1} - f_1\\ J_{ay}\dot{q}_a = T_{e2} - B_2\dot{v}_2 - T_{c2} - f_2 \end{cases} \tag{8}$$

where T_{el} is the motor electromagnetic torque, B_l is the viscous friction coefficient, and the subscripts $l = 1,2$ represent the parameters related to the yaw and pitch gimbals, respectively.

In practical engineering, it is always feasible to get the nominal values J_{ol} of the total moments of inertial for the yaw and pitch gimbals. That is, $J_{o1} = \bar{J}_{az} + \bar{J}_{kz}$ and $J_{o2} = \bar{J}_{ay}$, where $\bar{J}_{az}, \bar{J}_{kz}$, and $\bar{J}_{ay}$ are the nominal values of J_{az}, J_{kz}, and J_{ay}, respectively. As such, the parameter variations of the moments of inertial can be expressed as $\Delta J_1 = J_{km} - J_{o1}$ and $\Delta J_2 = J_{ay} - J_{o2}$. In addition, it can be calculated from (1) that the angular rates of two motors satisfy

$$\dot{v}_1 = r_a - \Omega_1, \dot{v}_2 = q_a - \Omega_2 \tag{9}$$

where

$$\Omega_1 = r_a - r_a\sec v_2 + p_k\tan v_2 + r, \Omega_2 = q_k.$$

Combining with (9), the dynamic model (8) can be rearranged as follows:

$$J_{ol}\dot{\omega}_l = T_{el} - B_l\omega_l - F_l, \quad l = 1,2 \tag{10}$$

where $\omega_1 = r_a, \omega_2 = q_a$, and $F_l = T_{cl} + f_l + \Delta J_l r_a - B_l\Omega_l$.

System (10) reveals that if the cross-couplings T_{cl} is lumped into the total uncertainties F_l, the 2-DOF ISP system is taken to be decoupled and two independent single-input and single-output (SISO) systems can be obtained.

2.2. Cascade control models under FOC structure

The actuators employed here are two surface-mounted PMSMs, which are utilized to generate the electromagnetic torques T_{el}. Suppose that the three-phase stator windings of the PMSM are sinusoidally distributed in space, the model of the PMSM servo system can be given in the explicit form as [28]

$$\begin{cases} \dot{i}_{dl} = -\dfrac{R_{sl}}{L_{dl}}i_{dl} + n_{pl}i_{ql}\dot{v}_l + \dfrac{u_{dl}}{L_{dl}}\\ \dot{i}_{ql} = -\dfrac{R_{sl}}{L_{ql}}i_{ql} - n_{pl}i_{dl}\dot{v}_l + \dfrac{n_{pl}\phi_{vl}}{L_{ql}}\dot{v}_l + \dfrac{u_{ql}}{L_{ql}} \end{cases} \quad l = 1,2 \tag{11}$$

where the i_{dl} and i_{ql} represent the stator currents, L_{dl} and L_{ql} are the inductances, u_{dl} and u_{ql} are the stator voltages, and R_{sl}, n_{pl}, and ϕ_{vl} are the stator resistance, the number of pole pair, and the rotor flux linkage, respectively.

Furthermore, the electromagnetic torque can be calculated by

$$T_{el} = K_{fl}i_{ql}, \quad l = 1,2 \tag{12}$$

where $K_{fl} = 3n_{pl}[\phi_{vl} + (L_{dl} - L_{ql})i_{dl}]/2$ is the thrust coefficient.

Combining (10)–(12) together, the integrated dynamic model for the 2-DOF ISP system is established as follows:

$$\begin{cases} \dot{\omega}_l = \dfrac{K_{fl}}{J_{ol}}i_{ql} - \dfrac{B_l}{J_{ol}}\omega_l - d_{\omega l}\\ \dot{i}_{dl} = -\dfrac{R_{sl}}{L_{dl}}i_{dl} + n_{pl}\omega_l i_{ql} + \dfrac{u_{dl}}{L_{dl}} - d_{dl}\\ \dot{i}_{ql} = -\dfrac{R_{sl}}{L_{ql}}i_{ql} - n_{pl}\omega_l i_{dl} + \dfrac{n_{pl}\phi_{vl}}{L_{ql}}\omega_l + \dfrac{u_{ql}}{L_{ql}} - d_{ql} \end{cases} \quad l = 1,2 \tag{13}$$

where

$$d_{\omega l} = \frac{F_l}{J_{ol}}, d_{dl} = n_{pl}i_{ql}\Omega_l, d_{ql} = -n_{pl}i_{dl}\Omega_l + \frac{n_{pl}\phi_{vl}}{L_{ql}}\Omega_l$$

which indicates that the ISP system is subject to the matched and mismatched uncertainties.

To decouple the torque generation and magnetization functions in PMSM, the FOC technique is employed, for which the detailed control configuration can be referred to [29]. It should be pointed out that the outer loop here is the inertial stabilized loop rather than speed loop in comparison with the conventional PMSM drive system. Assume that ω_l^*, i_{dl}^*, and i_{ql}^* are the reference trajectories. Usually, i_{dl}^* is set to zero to maintain a constant flux operating condition. Define the tracking errors as $e_{\omega l} = \omega_l^* - \omega_l$, $e_{dl} = i_{dl}^* - i_{dl}$, and $e_{ql} = i_{ql}^* - i_{ql}$. Let $x_1 = e_{\omega 1}, \boldsymbol{x}_2 = [e_{d1}, e_{q1}]^{\mathrm{T}}, x_3 = e_{\omega 2}, \boldsymbol{x}_4 = [e_{d2}, e_{q2}]^{\mathrm{T}}, u_1 = i_{q1}^*, \boldsymbol{u}_2 = [u_{d1}, u_{q1}]^{\mathrm{T}}, u_3 = i_{q2}^*, \boldsymbol{u}_4 = [u_{d2}, u_{q2}]^{\mathrm{T}}$. Then, the error dynamics of system (13) with cascaded form is presented as

$$\begin{cases} \dot{x}_1 = g_1(x_1) + b_1(x_1)u_1 + d_1(x_1) + h(x_1, \boldsymbol{x}_2)\\ \dot{\boldsymbol{x}}_2 = \boldsymbol{g}_2(\boldsymbol{x}_2) + \boldsymbol{b}_2(\boldsymbol{x}_2)\boldsymbol{u}_2 + \boldsymbol{d}_2(\boldsymbol{x}_2)\\ \dot{x}_3 = g_3(x_3) + b_3(x_3)u_3 + d_3(x_3) + h(x_3, \boldsymbol{x}_4)\\ \dot{\boldsymbol{x}}_4 = \boldsymbol{g}_4(\boldsymbol{x}_4) + \boldsymbol{b}_4(\boldsymbol{x}_4)\boldsymbol{u}_4 + \boldsymbol{d}_4(\boldsymbol{x}_4) \end{cases} \tag{14}$$

where

$$g_1(x_1) = \dot{\omega}_1^* + \frac{B_1}{J_{o1}}\omega_1, h(x_1, \boldsymbol{x}_2) = \frac{K_{f1}}{J_{o1}}e_{q1},$$
$$\boldsymbol{g}_2(\boldsymbol{x}_2) = [\dot{i}_{d1}^* + \frac{R_{s1}}{L_{d1}}i_{d1} - n_{p1}\omega_1 i_{q1},$$
$$\dot{i}_{q1}^* + \frac{R_{s1}}{L_{q1}}i_{q1} + n_{p1}\omega_1 i_{d1} - \frac{n_{p1}\phi_{v1}}{L_{q1}}\omega_1]^{\mathrm{T}},$$
$$g_3(x_3) = \dot{\omega}_2^* + \frac{B_2}{J_{o2}}\omega_2, h(x_3, \boldsymbol{x}_4) = \frac{K_{f2}}{J_{o2}}e_{q2},$$
$$\boldsymbol{g}_4(\boldsymbol{x}_4) = [\dot{i}_{d2}^* + \frac{R_{s2}}{L_{d2}}i_{d2} - n_{p2}\omega_2 i_{q2},$$
$$\dot{i}_{q2}^* + \frac{R_{s2}}{L_{q2}}i_{q2} + n_{p2}\omega_2 i_{d2} - \frac{n_{p2}\phi_{v2}}{L_{q2}}\omega_2]^{\mathrm{T}},$$
$$b_1(x_1) = -\frac{K_{f1}}{J_{o1}}, \boldsymbol{b}_2(\boldsymbol{x}_2) = \mathrm{diag}(-\frac{1}{L_{d1}}, -\frac{1}{L_{q1}}),$$
$$b_3(x_3) = -\frac{K_{f2}}{J_{o2}}, \boldsymbol{b}_3(\boldsymbol{x}_3) = \mathrm{diag}(-\frac{1}{L_{d2}}, -\frac{1}{L_{q2}}),$$
$$d_1(x_1) = d_{\omega 1}, \boldsymbol{d}_2(\boldsymbol{x}_2) = [d_{d1}, d_{q1}]^{\mathrm{T}},$$
$$d_3(x_3) = d_{\omega 2}, \boldsymbol{d}_4(\boldsymbol{x}_4) = [d_{d2}, d_{q2}]^{\mathrm{T}}.$$

Remark 1. System (14) reveals that the similar control structures can be obtained for the yaw and pitch gimbals. As such, the motions of the yaw and pitch axes can be separately controlled. Obviously, for each decoupled system, a stabilized loop and a current loop are involved. This treatment can also be understood from the perspective of backstepping design techniques [30], where u_1 and u_3 are the selected virtual control variables. To eliminate the side effects caused by the mismatched and matched uncertainties, this paper explores a continuous finite-time sliding mode control approach with cascaded control structure for the ISP system. The control objective is to ensure that the output tracking errors $x_1 = e_{\omega_1}$ and $x_3 = e_{\omega_2}$ can converge to zero in finite time.

3. System controller design

Since the yaw and pitch gimbals have the similar control process, the detailed design process is described step-by-step by taking the yaw gimbal as an example. The system dynamics for the yaw gimbal system are expressed as

$$\dot{x}_1 = g_1(x_1) + b_1(x_1)u_1 + d_1(x_1) + h(x_1, \boldsymbol{x}_2) \tag{15}$$
$$\dot{\boldsymbol{x}}_2 = \boldsymbol{g}_2(\boldsymbol{x}_2) + \boldsymbol{b}_2(\boldsymbol{x}_2)\boldsymbol{u}_2 + \boldsymbol{d}_2(\boldsymbol{x}_2) \tag{16}$$

To begin with, some essential assumptions are firstly made as follows:

Assumption 1. The derivative of the lumped uncertainty $d_1(x_1)$ in subsystem (15) exists and has a known Lipschitz constant L.

Assumption 2. The derivatives of the lumped uncertainties $\boldsymbol{d}_2(\boldsymbol{x}_2)$ in subsystem (16) are bounded by positive constants, i.e., $|\dot{d}_{d1}| \leq \delta_{id}$, $|\dot{d}_{q1}| \leq \delta_{iq}$.

Assumptions 1–2 mean that the change rate of the disturbance is always limited in the physical world, which is a general one made in the continuous sliding mode control design [31,32].

3.1. Controller design for stabilized loop

Let z_0, z_1, and z_2 be the estimates of $\omega_1, d_1(x_1)$, and $\dot{d}_1(x_1)$, respectively. Motivated by [26], a FTDO for the lumped disturbance estimation is designed as

$$\begin{cases} \dot{z}_0 = v_0 - \frac{B_1}{J_{o1}}\omega_1 + \frac{K_{f1}}{J_{o1}}i_{q1} := f_0(t, z_0, z_1, z_2), \\ \dot{z}_1 = v_1 := f_1(t, z_0, z_1, z_2), \\ \dot{z}_2 = v_2 := f_2(t, z_0, z_1, z_2), \\ v_0 = -\lambda_0 L^{1/3}|z_0 - \omega_1|^{2/3}\mathrm{sign}(z_0 - \omega_1) + z_1, \\ v_1 = -\lambda_1 L^{1/2}|z_1 - v_0|^{1/2}\mathrm{sign}(z_1 - v_0) + z_2, \\ v_2 = -\lambda_2 L\mathrm{sign}(z_2 - v_1), \end{cases} \tag{17}$$

where $\lambda_i > 0, i = 1, 2, 3$ are coefficients of the observer to be designed and v_0, v_1, and v_2 are the intermediate variables.

Remark 2. The selections of parameters λ_i of (17) are referred to [19]. A possible parameters selection here is $\lambda_0 = 2, \lambda_1 = 1.5, \lambda_2 = 1.1$. When taking a larger value of L, the faster convergence rate of the observer can be obtained. In this view, the fast time-varying disturbance could be estimated by increasing L. However, this induces the amplification of the measurement noise unavoidably. In general, it is always possible to select a proper value L such that a compromise between the disturbance rejection performance and measurement noise attenuation could be achieved.

Remark 3. In comparison with the DOBs introduced in [23,25], the designed FTDO is not only adequate for the fast time-varying disturbance estimation but also guarantees the finite-time observation [19,26].

For the stabilized loop subsystem (15), the sliding mode variable is defined as $\sigma = x_1$, the proposed IMSTW controller is designed as

$$\begin{aligned} u_1 &= -b_1(x_1)^{-1}(u_{stw} + u_{com}), \\ u_{stw} &= g_1(x_1) + k_1|\sigma|^{\frac{1}{2}}\mathrm{sign}(\sigma) + k_2\int_0^t \mathrm{sign}(\sigma)d\tau, \\ u_{com} &= \hat{d}_1 \end{aligned} \tag{18}$$

where $k_1, k_2 > 0$ are the design parameters, and $\hat{d}_1(x_1) = z_1$ is given by the FTDO (17).

Remark 4. The proposed control method (18) is continuous such that the chattering phenomenon is effectively attenuated. Compared to the general SMC method where the boundary layer technique is usually adopted to reduce the chattering effect [14], the non-smooth functions $|x|^{\alpha}\mathrm{sign}(x)$ and $\int_0^t \mathrm{sign}(x)d\tau$ associating with the disturbance estimate are utilized to design the control law. In fact, using the integral of the high-frequency switching function $\mathrm{sign}(\sigma)$ to realize the chattering attenuation is extensively used in the field of sliding mode control. The key philosophy is to make the switching term "hidden" under the integral. This attractive idea has also been applied in many research articles on the design of continuous sliding mode control [14,32,31].

Remark 5. The selections of the feedback control gains k_1 and k_2 here do not have to depend on the boundary of $d_1(x_1)$, which can be chosen relative small even in the presence of the unknown cross-couplings and external disturbances. The overlarge control gains may result in the undesirable dynamic performances such as severe steady-state fluctuations and excessive transient overshoot, and this is avoidless in the general SMC [14] and STW control [21] methods.

3.2. Controller design for current loop

For the current loop subsystem (16), note that $\boldsymbol{g}_2(\boldsymbol{x}_2)$ involves the derivative term of the control input $\dot{i}_{q1}^*$, which can be calculated

by

$$\dot{i}_{q1}^{*} = -b_1^{-1}(x)(\frac{du_{stw}}{dt} + \frac{du_{com}}{dt}) = \frac{dg_1(x_1)}{dt} + \frac{k_1}{2}|\sigma|^{-\frac{1}{2}} + k_2\text{sign}(\sigma) + \dot{\hat{d}}_1.$$

It is obvious seen that while the sliding mode σ reaches the equilibrium point, there exists a singularity. Moreover, $\dot{\hat{d}}_1$ cannot be obtained directly as well. To cover with the problems, the first-order differentiator (FOD) introduced in [19] is adopted to compute the derivative of i_{q1}^{*}, which is designed as

$$\begin{cases} \dot{\xi}_0 = \zeta_0 = -\epsilon_0|\xi_0 - i_{q1}^{*}|^{1/2}\text{sign}(\xi_0 - i_{q1}^{*}) + \xi_1, \\ \dot{\xi}_1 = -\epsilon_1\text{sign}(\xi_1 - \zeta_0) \end{cases} \tag{19}$$

where ξ_0, ξ_1, and ζ_0 are the system states, ϵ_0 and ϵ_1 are the positive design constants using to regulate the convergence rate of the differentiator. Then, it can be obtained that $\dot{i}_{q1}^{*} = \zeta_0 + \delta$ where δ is the estimated error of the differentiator. Thus $\boldsymbol{g}_2(\boldsymbol{x}_2)$ in (16) can be modified as

$$\boldsymbol{g}_2(\boldsymbol{x}_2) = [\frac{R_{s1}}{L_{d1}}i_{d1} - n_{p1}\omega_1 i_{q1}, \zeta_0 + \delta + \frac{R_{s1}}{L_{q1}}i_{q1} + n_{p1}\omega_1 i_{d1} - \frac{n_{p1}\phi_{v1}}{L_{q1}}\omega_1]^{\mathrm{T}}. \tag{20}$$

It follows from [19] that $\delta \equiv \dot{\delta} \equiv 0$ after finite time.

Borrowed the idea presented in [21], for the current loop subsystem, the STW control law is designed as

$$\boldsymbol{u}_2 = -\boldsymbol{b}_2(\boldsymbol{x}_2)^{-1}[\hat{\boldsymbol{g}}_2(\boldsymbol{x}_2) + \boldsymbol{M}\text{sig}(\boldsymbol{x}_2) + \boldsymbol{N}\boldsymbol{r}(\boldsymbol{x}_2)] \tag{21}$$

where

$$\text{sig}(\boldsymbol{x}_2) = \left[|e_{d1}|^{\frac{1}{2}}\text{sign}(e_{d1}), |e_{q1}|^{\frac{1}{2}}\text{sign}(e_{q1})\right]^{\mathrm{T}},$$

$$\boldsymbol{r}(\boldsymbol{x}_2) = \left[\int_0^t \text{sign}(e_{d1})d\tau, \int_0^t \text{sign}(e_{q1})d\tau\right]^{\mathrm{T}},$$

$$\hat{\boldsymbol{g}}_2(\boldsymbol{x}_2) = [\frac{R_{s1}}{L_{d1}}i_{d1} - n_{p1}\omega_1 i_{q1}, \zeta_0 + \frac{R_{s1}}{L_{q1}}i_{q1} + n_{p1}\omega_1 i_{d1} - \frac{n_{p1}\phi_{v1}}{L_{q1}}\omega_1]^{\mathrm{T}},$$

and $\boldsymbol{M} = \text{diag}(m_1, m_2), \boldsymbol{N} = \text{diag}(n_1, n_2)$ are the gain matrices. For the parameter selections of $\boldsymbol{M}$ and $\boldsymbol{N}$, the following conditions should be satisfied:

$$m_1 = 1.5\sqrt{\delta_{id}}, m_2 = 1.5\sqrt{\bar{\delta}_{iq}}, n_1 = 1.1\delta_{id}, \ n_2 = 1.1\bar{\delta}_{iq} \tag{22}$$

where $\bar{\delta}_{iq} = \delta_{iq} + \delta_u$ and δ_u is the upper bound of $|\dot{\delta}|$. Generally, δ_u is a small positive value in actual applications. Under the condition (22), the subsystem (16) is finite-time stable if the controller is designed as (21), i.e., $\boldsymbol{x}_2 \equiv 0$ after a finite time T_i. This attractive property is guaranteed by Lemma 2 below.

Remark 6. For the current loop, the traditional STW controller is directly employed instead of the proposed IMSTW control method. There are mainly two reasons for this choice. First, the control period (100 μs) of the current loop is much less than that of the stabilized loop (500 μs). Although the IMSTW control method achieves better performance as stated in Remark 5, a series of differential equations are expected to be solved in real time for the reconstruction of the disturbance $\boldsymbol{d}_2(\boldsymbol{x}_2)$, which inevitably increases the computational burden. Second, different from the complicated disturbance $d_1(x_1)$, the knowledge of $\boldsymbol{d}_2(\boldsymbol{x}_2)$ is relatively easy to obtain in the practical engineering, which means the feedback control gains do not have to be chosen conservatively.

The configuration of the proposed control method is depicted in Fig. 3.

3.3. Stability analysis of the closed-loop cascaded system

The stability of the closed-loop system is analyzed in this section.

Lemma 1 ([26]). *Suppose that the errors are defined as $e_0 = z_0 - \omega_1$, $e_1 = z_1 - d_1$, and $e_2 = z_2 - \dot{d}_1$. Then the observer estimation errors of the FTDO (17) are governed by*

$$\begin{cases} \dot{e}_0 = -\lambda_0 L^{1/3}|e_0|^{2/3}\text{sign}(e_0) + e_1, \\ \dot{e}_1 = -\lambda_1 L^{1/2}|e_1 - \dot{e}_0|^{1/2}\text{sign}(e_1 - \dot{e}_0) + e_2, \\ \dot{e}_2 \in -\lambda_2 L\text{sign}(e_2 - \dot{e}_1) + [-L, L]. \end{cases} \tag{23}$$

For error dynamics (23), there exists a time constant $T_f \in R^+$, for $\forall t > T_f$, $e_0 = e_1 = e_2 = 0$, that is the disturbance estimation errors converge to zero in finite time.

Lemma 2 ([33]). *Consider the following system*

$$\begin{cases} \dot{x}_1 = -k_1|x_1|^{1/2}\text{sign}(x_1) + x_2, \\ \dot{x}_2 = -k_2\text{sign}(x_1) + d \end{cases} \tag{24}$$

Suppose that the disturbance $|d| < \Delta$, if k_1 and k_2 are selected as $k_1 = 1.5\sqrt{\Delta}$ and $k_2 = 1.1\sqrt{\Delta}$, then $x_1 = \dot{x}_1 = 0$ are achieved in finite time. The settling time T is given by

$$T \le \frac{2\lambda_{\max}\{P\}}{\lambda_{\min}^{\frac{1}{2}}\{P\}\lambda_{\min}\{Q\}}V^{\frac{1}{2}}(x_1(0)) \tag{25}$$

where the quadratic function $V = \xi^{\mathrm{T}}P\xi$ with $\xi^{\mathrm{T}} = [|x_1|^{\frac{1}{2}}\text{sign}(x_1), x_2]$, P is a constant, symmetric and positive definite matrix, and Q denotes some symmetric and positive definite matrix satisfying the Lyapunov function $A^{\mathrm{T}}P + PA = -Q$, in which

$$A = \begin{bmatrix} -\frac{1}{2}k_1 & \frac{1}{2} \\ -k_2 & 0 \end{bmatrix}$$

Particularly, if $d = 0$, k_1 and k_2 only need to be chosen as the positive constants.

Lemma 3 ([34]). *The following time-varying cascaded system*

$$\begin{cases} \dot{x}_1 = f_1(t, x_1) + g(t, x_1, x_2), \\ \dot{x}_2 = f_2(t, x_2) \end{cases} \tag{26}$$

is finite-time stable if the following conditions are satisfied:

1. *The subsystems $\dot{x}_1 = f_1(t, x_1)$ and $\dot{x}_2 = f_2(t, x_2)$ are finite-time stable.*
2. *For any fixed and bounded x_2, there exists a positive definite and radially unbounded finite-time bounded (FTB) function $B(t, x_1)$, which satisfies*

   $$\dot{B}(t, x_1) \le \beta B(t, x_1) + L_B$$

   where β and L_B are positive constants.

Theorem 1. *Under Assumptions 1–2, for the cascaded system (15)–(16), if the disturbance observer is designed as (17), the control laws for the stabilized loop and current loop are designed as (18) and (21), respectively, with the proper selections of the control gains $k_1, k_2, \boldsymbol{M}, \boldsymbol{N}$, the following statements hold:*

1. *The cascaded system (15)–(16) is FTS.*
2. *The system output ω_1 converges to the desired value ω_1^{*} in finite time even in the presence of the multiple disturbances.*

Proof. By substituting the control laws (18) and (21) into systems (15) and (16), respectively, the following cascaded system can be derived:

$$\dot{x}_1 = f_1(t, x_1) + g(t, \boldsymbol{e}, \boldsymbol{x}_2), \tag{27}$$

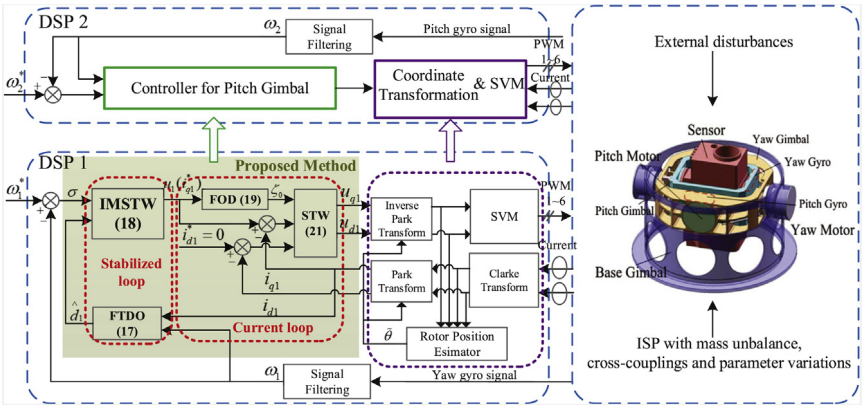

Fig. 3. Configuration of 2-DOF ISP with proposed control method under the FOC structure.

$$\dot{\boldsymbol{x}}_2 = \boldsymbol{f}_2(t, \boldsymbol{x}_2), \tag{28}$$

$$\dot{\boldsymbol{e}} = \boldsymbol{f}(t, \boldsymbol{e}), \tag{29}$$

where

$$f_1(t, x_1) = -k_1|\sigma|^{\frac{1}{2}}\text{sign}(\sigma) - k_2\int_0^t \text{sign}(\sigma)d\tau,$$

$$g(t, \boldsymbol{e}, \boldsymbol{x}_2) = -e_1 + K_{f1}e_{\omega 1}/J_{o1},$$

$$\boldsymbol{f}_2(t, \boldsymbol{x}_2) = -\boldsymbol{M}\text{sig}(\boldsymbol{x}_2) - \boldsymbol{N}\boldsymbol{r}(\boldsymbol{x}_2) + \bar{\boldsymbol{d}}_2(t, \boldsymbol{x}_2),$$

$$\bar{\boldsymbol{d}}_2(t, \boldsymbol{x}_2) = \boldsymbol{d}_2(t, \boldsymbol{x}_2) + \boldsymbol{g}_2(\boldsymbol{x}_2) - \hat{\boldsymbol{g}}_2(\boldsymbol{x}_2),$$

and $\dot{\boldsymbol{e}} = \boldsymbol{f}(t, \boldsymbol{e})$ denotes the estimation error Eq. (23).

The stability analysis is divided into three steps. First, the subsystems (28) and (29) are finite-time stable (FTS) when $t > \max(T_i, T_f)$. Second, the bounded estimation error e_1 and state error $e_{\omega 1}$ will not drive the sliding mode variable σ to the infinity in any time interval $[0, \max(T_i, T_f)]$. Finally, the finite-time stability of the subsystem $\dot{x}_1 = f_1(t, x_1)$ is given.

Step 1: If the parameter matrices $\boldsymbol{M}$ and $\boldsymbol{N}$ are chosen as (22), it can be concluded Lemma 2 that subsystem (28) is FTS when $t > T_i$. From Lemma 1, we can also obtain that subsystem (29) is FTS when $t > T_f$. That is, for $\forall t > \max(T_i, T_f)$, $e_1 \equiv e_{\omega 1} \equiv 0$ and for $\forall t \le \max(T_i, T_f)$, e_1 and $e_{\omega 1}$ are always bounded by the positive constants $e_1^{\max}$ and $e_{\omega 1}^{\max}$, respectively.

Step 2: Define a finite-time bounded (FTB) function [34] as $V_1 = 1/2\sigma^2$, for $\forall t \le \max(T_i, T_f)$. Taking the derivative of V_1 yields

$$\begin{aligned}\dot{V}_1 &= \sigma\dot{\sigma}\\ &= -k_1|\sigma|^{\frac{3}{2}} - k_2\sigma\int_0^t \text{sign}(\sigma)d\tau - e_1\sigma + \frac{K_{f1}}{J_{o1}}e_{\omega 1}\sigma\\ &\le \left(k_2 t - e_1 + \frac{K_{f1}}{J_{o1}}e_{\omega 1}\right)\sigma\\ &\le \frac{1}{2}\sigma^2 + \frac{1}{2}\left(\frac{K_{f1}}{J_{o1}}e_{\omega 1} - e_1 + k_2 t\right)^2\\ &\le K_{v1}V_1 + L_{v1},\end{aligned} \tag{30}$$

where $K_{v1} = 1$ and $L_{v1} = 1/2[K_{f1}e_{\omega 1}^{\max}/J_{o1} + e_1^{\max} + k_2\max(T_i, T_f)]^2$ are bounded constants. Solving the inequality (30), we have

$$V_1(t) \le \frac{L_{v1}}{K_{v1}} + \left(V_1(\sigma(0)) - \frac{L_{v1}}{K_{v1}}\right)e^{K_{v1}t},\ t \le \max(T_i, T_f). \tag{31}$$

That is, σ is bounded.

Step 3: When $t > \max(T_i, T_f)$, subsystem (27) reduces to $\dot{\sigma} = f_1(t, \sigma)$, i.e.,

$$\sigma = -k_1|\sigma|^{\frac{1}{2}}\text{sign}(\sigma) - k_2\int_0^t \text{sign}(\sigma)d\tau. \tag{32}$$

From Lemma 2, it can be concluded that σ will converge to zero in finite time T_s, where

$$T_s \le \frac{2\lambda_{\max}\{P\}}{\lambda_{\min}^{\frac{1}{2}}\{P\}\lambda_{\min}\{Q\}}V_2^{\frac{1}{2}}(\sigma(0)) + \max(T_i, T_f).$$

With *Steps 1–3*, we can obtain that the cascaded system (15)–(16) is FTS from Lemma 3. That is, the system output ω_1 can converge to the desired value ω_1^* in finite time even in the presence of the disturbances $d_1(x_1)$ and $\boldsymbol{d}_2(\boldsymbol{x}_2)$. This completes the proof.

3.4. Digital implementation

In order to implement the algorithms (18) and (21) in a DSP model, the continuous control laws should be discretized first which is different from the design within the simulation environment in MATLAB software. Suppose that the sampling period (interrupt interval) of the control system is h. The discrete version of a continuous signal $x(t)$ can be $x(kh)$, where $k \in N^+$. For a differential signal $\dot{x}(t)$, the general discrete version is $[x((k+1)h) - x(kh)]/h$ named as Euler discretization, which is a well known and widely used approximate method. The higher solving accuracy will be obtained if h is relatively small. However, for the motion control system, due to the limited switching frequency of the power driver, h cannot be chosen too small. To improve the computational accuracy, the Runge–Kutta method introduced in [35] is employed for the computation of the nonlinear differential equations (17) and (19). A 4-stage explicit Runge–Kutta algorithm for the FTDO (17) can be expressed as follows

$$\begin{aligned}z_m((k+1)h) &= z_m(kh) + \sum_{i=1}^{4} b_i k_{mi},\\ k_{mi} &= hf_m(\bar{t}, \bar{z}_0, \bar{z}_1, \bar{z}_2)\end{aligned} \tag{33}$$

where

$$\bar{t} = t(kh) + c_i h,\ c_i = \sum_{j=1}^{4} a_{ij},\ \bar{z}_m = z_m(kh) + h\sum_{j=1}^{i-1} a_{ij}k_{mj}$$

for $m = 0, 1, 2$ and $i = 1, \ldots, 4$. An alternative parameters selection here for $a_{ij}(1 < j < i)$, b_i and c_i are $a_{31} = a_{41} = a_{42} = 0$, $a_{21} = a_{32} = 1/2$, $a_{43} = 1$, $b_1 = 1/6$, $b_2 = b_3 = 1/3$, $b_4 = 1/6$, $c_1 = 0$, $c_2 = c_3 = 1/2$, and $c_4 = 1$. A similar process can be performed for (19).

4. Experimental results

To investigate the effectiveness of the proposed continuous finite-time SMC method, experimental studies on the ISP system

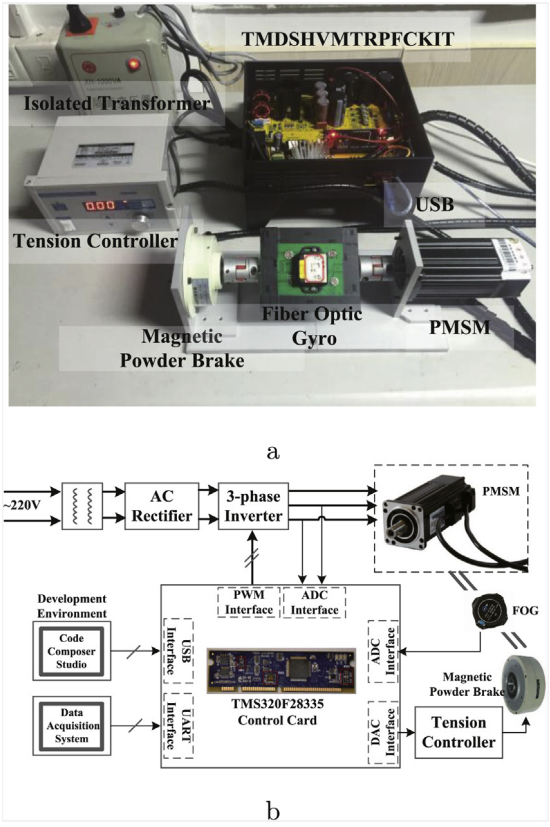

Fig. 4. DSP-based control system: (a) Experimental setup and (b) Block diagram.

are performed in this section. Since the cross-coupled system can be considered as decoupled by treating the multiple disturbances as the lumped uncertainty, a single-axis stabilized platform coupled with the magnetic powder brake is built up to imitate the 2-DOF gimbal system, as shown in Fig. 4. The magnetic powder brake is utilized to generate the multiple disturbances, which is controlled by a tension controller through the external input analog interface. The platform takes PMSM as an actuator, which is driven by a controller TMDSHVMTRPFCKIT provided by Texas Instruments. And the proposed control algorithm is implemented on the DSP TMS320F28335 with a clock frequency of 150 MHz. The fiber optic gyro (FOG) is fixed on the platform, used for the angular rates measurements for pitch and yaw channels, and the analog–digital conversion (ADC) for the gyro sensor signal is realized by the chip AD7656 with a resolution of 16 bits. An isolated transformer is also adopted to enhance the system security for experimental tests. Three-phase currents are measured by the precision resistors voltage divider and the RC low-pass filter is utilized to improve the signal-to-noise ratio. In addition, a host computer is utilized to realize the C-program development and data acquisition via USB and UART communication, respectively. The parameters of the adopted PMSM are listed in Table 1 and the nominal value of the total moment of inertial is 0.0925 kg m^2.

4.1. Comparative experimental verification

The traditional PI control and CSMC put forward by [17] are employed for both the stabilized loop and the current loop controller for the performance comparison with the proposed IMSTWs–STWc method, where the subscripts s and c denote the stabilized loop and the current loop, respectively. The different control schemes are presented as follows:

Table 1
Parameters of the PMSM.

Parameters	Meaning	Value
P	Rated Power	400 W
U	Rated Voltage	200 V
I_N	Rated Current	2.8 A
n_p	Number of Pole-pairs	4
R_s	Armature Resistance	1.52 Ω
L_d&L_q	Stator Inductance	0.004 H
B	Viscous Damping Coefficient	7.4×10^{-5} N m s/rad
ϕ_v	Rotor Flux	0.0931 wb
T_N	Rated Torque	2.0 N m

Table 2
Control parameters of different controllers.

Controllers	Parameters
PIs–PIc	$K_{ps}=25, K_{is}=1.25, \boldsymbol{K_{pc}}=\text{diag}(5.5, 9.5), \boldsymbol{K_{ic}}=\text{diag}(1.35, 2.15)$
CSMCs–CSMCc	$k_1=25, k_2=1.25, \boldsymbol{M}=\text{diag}(5.5, 9.5), \boldsymbol{N}=\text{diag}(1.35, 2.15)$
IMSTWs–STWc	$k_1=25, k_2=1.25, L=10, \boldsymbol{M}=\text{diag}(5.5, 9.5), \boldsymbol{N}=\text{diag}(1.35, 2.15)$

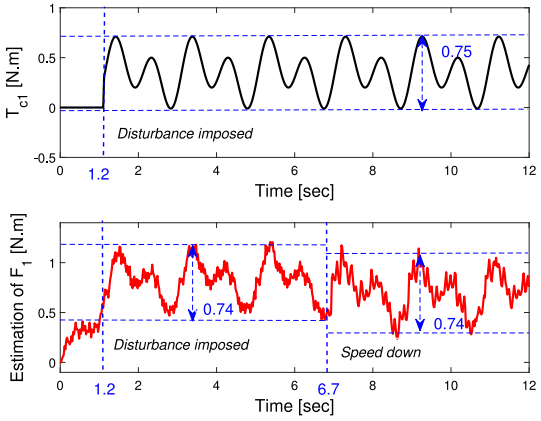

Fig. 5. Estimation results of the FTDO in the experiment.

(1) PIs–PIc:

$$\begin{aligned} u_1 &= -b_1(x_1)^{-1}\Big(K_{ps}x_1 + K_{is}\int_0^t x_1 d\tau\Big), \\ \boldsymbol{u}_2 &= -\boldsymbol{b}_2(\boldsymbol{x}_2)^{-1}\Big(\boldsymbol{K}_{pc}\boldsymbol{x}_2 + \boldsymbol{K}_{ic}\int_0^t \boldsymbol{x}_2 d\tau\Big) \end{aligned} \tag{34}$$

where K_{ps}, K_{is} are the control gains for the stabilized loop and $\boldsymbol{K}_{pc}, \boldsymbol{K}_{ic}$ are the control gain matrices for the current loop.

(2) CSMCs–CSMCc:

$$\begin{aligned} u_1 &= -b_1(x_1)^{-1}\big[g_1(x_1) + k_1|\sigma|^{\frac{1}{2}}\text{sign}(\sigma) + k_2\sigma\big], \\ \boldsymbol{u}_2 &= -\boldsymbol{b}_2(\boldsymbol{x}_2)^{-1}[\hat{\boldsymbol{g}}_2(\boldsymbol{x}_2) + \boldsymbol{M}\text{sig}(\boldsymbol{x}_2) + \boldsymbol{N}\boldsymbol{x}_2] \end{aligned} \tag{35}$$

where the definitions of the corresponding symbols can be referred to (18) and (21). Here, k_1, k_2, $\boldsymbol{M}$, $\boldsymbol{N}$ are the design parameters.

In the experiment, the switching frequency of the inverter IGBTs is chosen as 10 kHz, the sampling periods for the current loop and the stabilized loop are set as 100 μs and 500 μs, respectively, and the cross-coupling torque T_{c1} is generated by the magnetic powder brake and set as

$$T_{c1} = \begin{cases} 0, & t < 1.2 \text{ s}, \\ \big[0.15\sin(\pi t) + 0.25\sin(2\pi t) + 0.35\big] \text{ N m}, & t \geq 1.2 \text{ s} \end{cases} \tag{36}$$

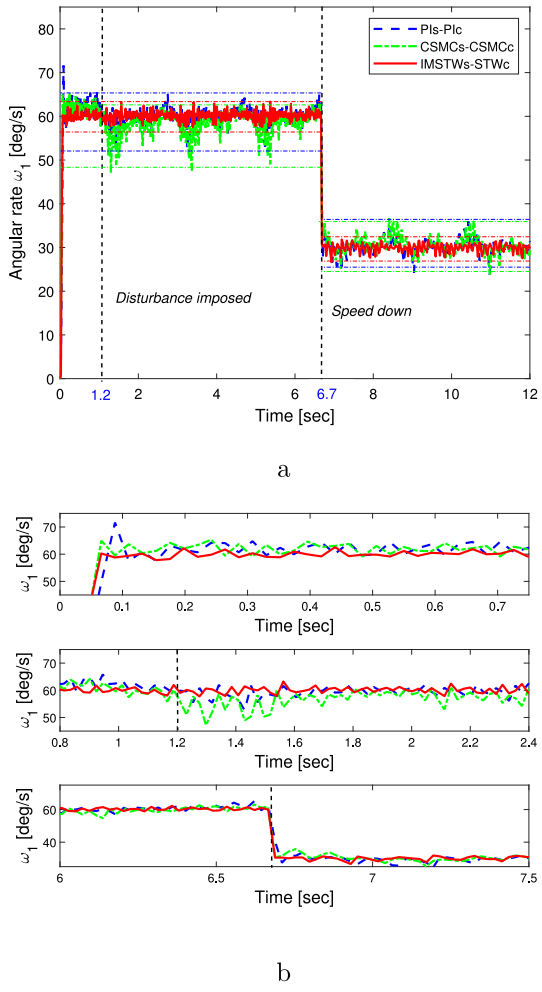

Fig. 6. Response curves of the angular rate under three different control schemes: (a) Angular rate and (b) Zoom-in plot of (a).

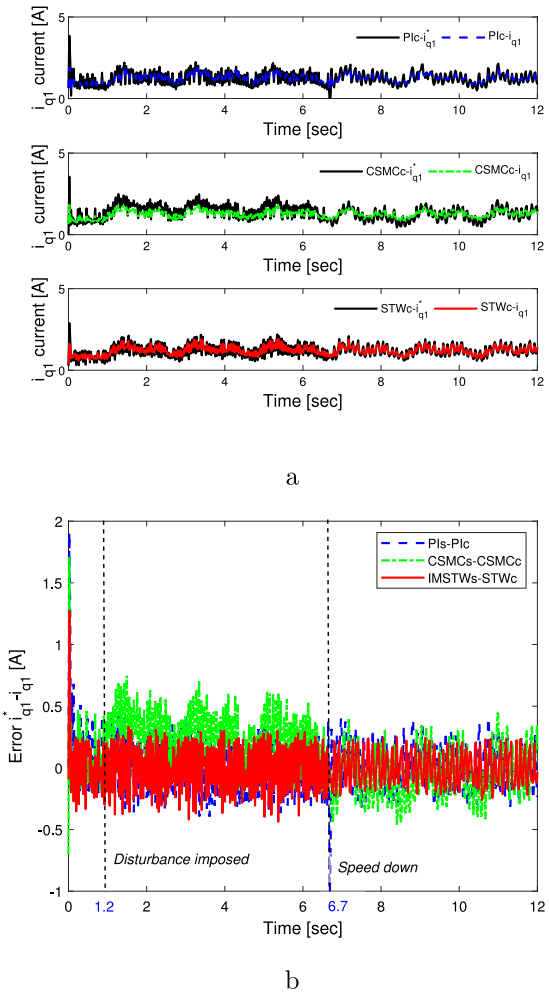

Fig. 7. Response curves of the q-axis current under three different control schemes: (a) q-axis current and (b) Tracking error.

The reference signal is changed from $\omega_1^* = 60$ deg/s to $\omega_1^* = 30$ deg/s at 6.7 s. For convenience, the parameters of three different control schemes are listed in Table 2.

Fig. 5 shows the disturbance estimation results of the FTDO. Note that F_1 involves the parameter uncertainties and friction torque besides the cross-couplings. If the constant competent of F_1 is removed, we can observe that the periodic competent caused by the cross-coupling torque T_{c1} is estimated accurately (with the peak-to-peak value of 0.74 N m).

Figs. 6–8 show that the proposed IMSTWs–STWc control obtains much more outstanding performance in terms of both the transient and steady state natures when compared with the PI control and CSMC methods. From Figs. 6b and 7b, it shows that the proposed method achieves almost the same response as that of CMSC method when $t < 1.2$ s, which verifies the nominal performance recovery ability of the proposed method. After the external disturbance is imposed, the tracking performance of the CSMC deteriorates seriously due to the existence of uncertainties. Although the role of integral term in PI controller is to eliminate the steady-state error of the first-order closed-loop system, the high-gains are always required to be selected for the suppression of time-varying disturbance. However, it often causes the undesirable noise and transient overshoot.

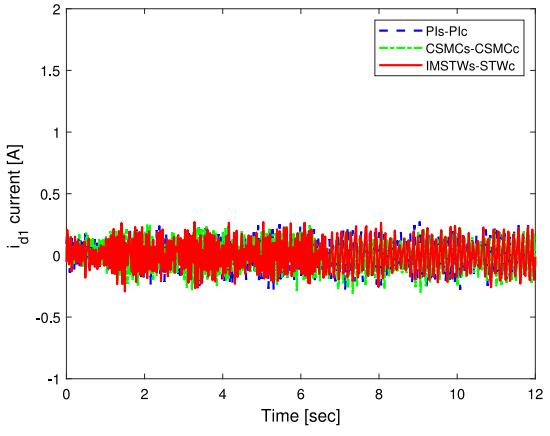

Fig. 8. Response curves of the d-axis current under three different control schemes.

4.2. Steady-State fluctuations reduction

Fig. 9 presents the comparative experiment results between the proposed method and the general STW method. It can be observed that the proposed method obtains the smaller steady-state fluctuation without sacrificing the disturbance rejection performance even by selecting the relative small control gains. As stated in

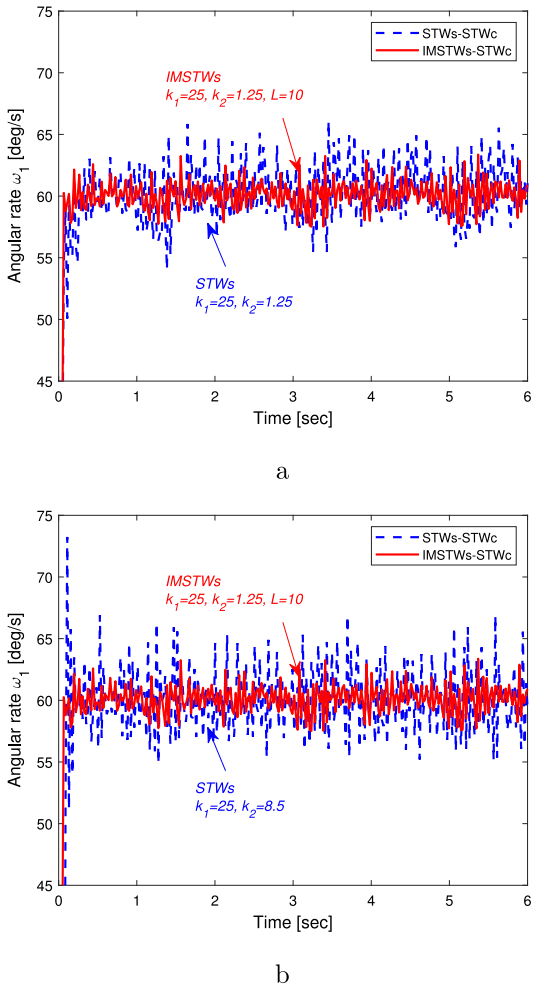

Fig. 9. Response curves of the angular rate with different control gains: (a) Same control gains and (b) Different control gains.

Remark 5, the disturbance can hardly be obtained as a priori in the application such that the control gains are always selected to be more conservative in the STW method. As shown in Fig. 9b, the overlarge control gain k_2 leads to the severely chattering and large steady-state fluctuation. The problem may be addressed by increasing k_2, however, it is probably insufficient for the enhanced disturbance only with the fixed-gain, which can be verified by Fig. 9a.

5. Conclusion

In this paper, a continuous finite-time SMC approach has been investigated for the 2-DOF ISP system in the presence of the multiple disturbances. The cross-coupled system has been decoupled by treating the multiple disturbances as the lumped uncertainty which is precisely estimated and compensated by using a FTDO. It has been shown that the resulting controller ensures the finite-time convergence of the output as well as the chattering attenuation through continuous control action. Moreover, by incorporating the disturbance estimation value, the feedback control gains can be reduced without sacrificing the disturbance rejection performance. Comparative experimental results confirm that the proposed control method exhibits better performances when compared with the traditional PI control and CSMC schemes.

Acknowledgments

This work was supported in part by the International Science & Technology Cooperation Program of China (grant no. 2015DFA10490), in part by the Primary Research & Development Plan of Jiangsu Province —Industry Prospects and Common Key Technologies (grant no. BE2016123), in part by the National Nature Science Foundation of China (grant nos. 61473080 and 61573099), in part by the Fundamental Research Funds for the Central Universities (grant nos. 2242016R30011 and 2242016K41067) and in part by the Postgraduate Research & Practice Innovation Program of Jiangsu Province (KYLX15_0213).

References

[1] Hilkert J. Inertially stabilized platform technology concepts and principles. IEEE Control Syst Mag 2008;28(1):26–46.
[2] Hurák Z, Řezáč M. Image-based pointing and tracking for inertially stabilized airborne camera platform. IEEE Trans Control Syst Technol 2012;20(5):1146–59.
[3] Moorty J, Marathe R. H∞ control law for line-of-sight stabilization for mobile land vehicles. Opt Eng 2002;41(11):2935–44.
[4] Řezáč M, Hurák Z. Structured mimo h∞ design for dual-stage inertial stabilization: case study for hifoo and hinfstruct solvers. Mechatronics 2013;23(8):1084–93.
[5] Li C, Jing W. Fuzzy pid controller for 2d differential geometric guidance and control problem. IET Control Theory Appl 2007;1(3):564–71.
[6] Abdo M, Vali A, Toloei A, Arvan M. Stabilization loop of a two axes gimbal system using self-tuning pid type fuzzy controller. ISA Trans 2014;53(2):591–602.
[7] Zhou X, Zhang H, Yu R. Decoupling control for two-axis inertially stabilized platform based on an inverse system and internal model control. Mechatronics 2014;24(8):1203–13.
[8] Fang J, Yin R, Lei X. An adaptive decoupling control for three-axis gyro stabilized platform based on neural networks. Mechatronics 2015;27(8):38–46.
[9] Ren X, Lewis F, Zhang J. Neural network compensation control for mechanical systems with disturbances. Automatica 2009;45(5):1221–6.
[10] Zhou X, Jia Y, Zhao Q, Cai T. Dual-rate-loop control based on disturbance observer of angular acceleration for a three-axis aerial inertially stabilized platform. ISA Trans 2016;63:288–98.
[11] Nichita C, Luca D, Dakyo B. Large band simulation of the wind speed for real time wind turbine simulators. IEEE Trans Energy Convers 2002;17(4):523–9.
[12] Ekstrand B. Equations of motion for a two-axes gimbal system. IEEE Trans Aerosp Electron Syst 2001;37(3):1083–91.
[13] Zhou X, Zhao B, Liu W, Yue H, Yu R, Zhao Y. A compound scheme on parameters identification and adaptive compensation of nonlinear friction disturbance for the aerial inertially stabilized platform. ISA Trans 2017;67:293–305.
[14] Shtessel Y, Edwards C, Fridman L, Levant A. Sliding mode control and observation. New York: Birkhäuser; 2014.
[15] Zou Y, Lei X. A compound control method based on the adaptive neural network and sliding mode control for inertial stable platform. Neurocomputing 2015;155:286–94.
[16] Mao J, Yang J, Li S, Yan Y, Li Q. Output feedback-based sliding mode control for disturbed motion control systems via a higher-order eso approach. IET Control Theory Appl 2018;12(15):2118–26.
[17] Yu S, Yu X, Shirinzaden B, Man Z. Continuous finite-time control for robotic manipulators with terminal sliding mode. Automatica 2005;41(11):1957–64.
[18] Jin M, Lee J, Ahn K. Continuous nonsingular terminal sliding-mode control of shape memory alloy actuators using time delay estimation. IEEE/ASME Trans Mechatronics 2015;20(2):899–909.
[19] Levant A. Higher-order sliding modes, differentiation and output-feedback control. Internat J Control 2003;76(9/10):924–41.
[20] Shtessel Y, Taleb M, Plestan F. A novel adaptive-gain supertwisting sliding mode controller: methodology and application. Automatica 2012;48(5):759–69.
[21] Davila J, Fridman L, Levant A. Second-order sliding-mode observer for mechanical systems. IEEE Trans Automat Control 2005;50(11):1785–9.
[22] Li S, Wu C, Sun Z. Design and implementation of clutch control for automotive transmissions using terminal-sliding-mode control and uncertainty observer. IEEE Trans Veh Technol 2016;65(4):1890–8.
[23] Han J. From pid to active disturbance rejection control. IEEE Trans Ind Electron 2009;56(3):900–6.
[24] Lei X, Zou Y, Dong F. A composite control method based on the adaptive rbfnn feedback control and the eso for two-axis inertially stabilized platforms. ISA Trans 2015;59:424–33.

[25] Godbole A, Kolhe J, Talole S. Performance analysis of generalized extended state observer in tackling sinusoidal disturbances. IEEE Trans Control Syst Technol 2013;21(6):2212–23.
[26] Shtessel Y, Shkolnikov I, Levant A. Smooth second-order sliding modes: Missile guidance application. Automatica 2007;43(8):1470–6.
[27] Yang J, Li S, Su J, Yu X. Continuous nonsingular terminal sliding mode control for systems with mismatched disturbances. Automatica 2013;49(7):2287–91.
[28] Liu H, Li S. Speed control for PMSM servo system using predictive functional control and extended state observer. IEEE Trans Ind Electron 2012;59(2):1171–83.
[29] Bernardes T, Montagner V, Gründling H, Pinheiro H. Discrete-time sliding mode observer for sensorless vector control of permanent magnet synchronous machine. IEEE Trans Ind Electron 2014;61(4):1679–91.
[30] Khalil H. Nonlinear systems. New Jersey: Prentice-Hall; 2002.
[31] Wang H, Pan Y, Li S, Yu H. Robust sliding mode control for robots driven by compliant actuators. IEEE Trans Control Syst Technol 2018. http://dx.doi.org/10.1109/TCST.2018.2799587.
[32] Feng Y, Han F, Yu X. Chattering free full-order sliding-mode control. Automatica 2014;50:1310–4.
[33] Moreno J, Osorio M. Strict lyapunov functions for the super-twisting algorithm. IEEE Trans Automat Control 2012;57(4):1035–40.
[34] Li S, Tian Y. Finite-time stability of cascaded time-varying systems. Internat J Control 2007;80(4):646–57.
[35] Anastassi Z, Simos T. An optimized runge-kutta method for the solution of orbital problems. J Comput Appl Math 2005;175(1):1–9.